C_i-Symmetry, [2 × 2] grid, square copper complex with the N^4,N^5-bis(4-fluorophenyl)-1*H*-imidazole-4,5-dicarboxamide ligand: structure, catecholase activity, magnetic properties and DFT calculations†

Arfa Parween[a], **Sumita Naskar**[bc], **Antonio J. Mota***[d], **Arturo Espinosa Ferao**[e], **Shyamal Kumar Chattopadhyay**[c], **Eric Rivière***[f], **William Lewis**[g] **and Subhendu Naskar***[a]

[a]*Department of Chemistry, Birla Institute of Technology, Mesra, Ranchi-835215, Jharkhand, India. E-mail: subnaskar@yahoo.co.in*

[b]*Department of Chemistry, RTC Institute of Technology, Anandi, Ormanjhi, Ranchi – 835219, Jharkhand, India*

[c]*Department of Chemistry, Indian Institute of Engineering Science and Technology – Shibpur, Howrah-711103, India*

[d]*Department of Inorganic Chemistry, Faculty of Sciences, University of Granada, Avda. Fuentenueva, s/n, 18002 Granada, Spain. E-mail: mota@ugr.es*

[e]*Department of Organic Chemistry, University of Murcia, Campus de Espinardo, 30100 Murcia, Spain*

[f]*Equipe Chimie Inorganique, Institut de Chimie Moléculaire et des Matériaux d'Orsay, Université Paris Sud, Bâtiment 420 – Rue du Doyen Georges Poitou, 91400 Orsay, France. E-mail: eric.riviere@u-psud.fr*

[g]*School of Chemistry, University of Nottingham, Nottingham NG7 2RD, UK*

Received 15th May 2017 , Accepted 3rd August 2017

First published on 3rd August 2017

A new square tetranuclear copper complex of formula **$Cu_4(LH)_4$·4DMF** with the dinucleating amide ligand N^4,N^5-bis(4-fluorophenyl)-1*H*-imidazole-4,5-dicarboxamide (LH_3) is reported herein. This ligand and the complex have been characterized by elemental analysis, FTIR, NMR, mass

and UV-visible spectroscopy, as well as magnetic and electrochemical measurements. The single crystal X-ray diffraction study showed each Cu centre in a distorted square pyramidal environment, the square plane being formed by the extended coordination of two sets (*N*,*N* and *N*,*O*) of donor atoms from pairs of different ligands. The Cu_4 unit has a C_i symmetry and crystallises in the $P\bar{1}$ space group in between DMF layers. The electronic spectrum of the complex exhibits a d–d transition at 676 nm. The complex also displays mild catecholase activity in DMF solution by using 3,5-di-*tert*-butylcatechol as substrate. Variable temperature magnetic measurements reveal an antiferromagnetic interaction between the copper centres with two different coupling constants of −143.4 and −169.0 cm^{-1}. DFT calculations made on a single Cu_4 unit from the crystal structure corroborated the antiferromagnetic coupling, the spin density of the lower-energy broken-symmetry state being consistent with an alternating +−+− singlet state operating at low temperature.

---

1. Introduction

Metal-assisted self-assembly processes constitute successful approaches to the synthesis of well defined, aesthetic, supramolecular structures from both biological[1–4] and synthetic[5–10] origins. Grid type complexes of five or six coordinate metal ions from first row transition metals display intriguing electronic and magnetic properties.[11,12] Electronically and magnetically active self-assembled metal containing motifs are promising candidates for the next generation of nanoscale electronic or spintronic devices.[13–15] In particular, square [$n \times n$] and rectangular [$m \times n$] grids, $m, n \leq 4$, are well documented as supramolecular devices for information storage and processing.[11,16] Designing of the grid like metal ion arrays is based on well directed coordination algorithm providing preferred coordination geometry of the metal ions and the ligand's donor sites. The deprotonated form of the amide functionality has good donor properties (either through oxygen or nitrogen atom) and can be synthesized easily. Thus, properly designed bis-amide ligands may provide suitable conformations to create a donor environment for adequate metals leading to square [2 × 2] grid-like structures. Use of amide ligands are advantageous over other systems due to reduction in the three-dimensional flexibility of the donor set while prohibiting the coordination of two amide groups to the same metal ion.[17]

Amides are biologically omnipresent functional groups. Metal–peptide complexes have a fascinating chemistry, being addressed by inorganic and biological chemists because of their bio-mimetic relevance.[18–25] Deprotonated form of amide ligands are capable to stabilize high oxidation state of metals and the resultant complexes often act as efficient oxidation catalysts.[26,27]

Catechol oxidase (CO), a type-III copper protein, catalyses the oxidation of *o*-diphenol to the corresponding quinone,[28,29] thereafter undergoing autopolymerisation to form melanin, a brown

coloured pigment. In this way CO protects damaged tissues of plants against pathogens or insects. X-ray crystal structure of CO from sweet potato (*Ipomoea batatas*), determined by T. Klabunde *et al.*,[30] reveals a dinuclear, hydroxo-bridged Cu_2 site, each copper being coordinated by three histidine nitrogen atoms. Therefore, a large number of dinuclear copper complexes[31–40] have been screened to study its CO activity. In this sense, molecular catalysts having more than two copper atoms, however, are very rare. Mazumdar *et al.* reported[41] a series of polymeric Cu^{II} complexes and their catecholase activities. Therefore, in order to achieve a deeper knowledge concerning the exact stereo-electronic requirements for catecholase activity and a better understanding of the catalytic process, more different polynuclear copper complexes should be explored.

In this work we report the synthesis, structure, variable temperature magnetic susceptibility measurement and catecholase activity of a new square Cu_4 complex with the dinucleating amide ligand N^4,N^5-bis(4-fluorophenyl)-1*H*-imidazole-4,5-dicarboxamide. Experimental magnetic behaviour has been supported by theoretical DFT calculations based on the broken-symmetry scheme.[42]

2. Experimental section

2.1 Materials

All chemicals and reagents were purchased from commercial sources, namely Fluka, Aldrich and E. Merck, and used without further purification. HPLC grade DMF was used for spectroscopic and electrochemical studies. All solvents were A.R. grade and used as received for synthetic work. Tetrabutylammonium perchlorate (TBAP), used for the electrochemical studies, was prepared according to the literature.[43]

2.2 Physical measurements

Infrared spectra were recorded as KBr pellets on a Shimadzu IR-Prestige21 spectrometer. Electronic spectra were recorded on a Perkin Elmer Lambda 750 Spectrophotometer. Elemental analyses were performed on Elementar Vario EL III C, H, N, S & O analyzer. Thermogravimetric analysis of the complex was executed in a DTG-60 (Shimadzu Corporation, Japan) from 30 to 800 °C. Electrochemical measurements of the ligand and complex were recorded in DMF containing 0.1 M TBAP as supporting electrolyte, using a CHI6003E potentiostat, glassy carbon working electrode, Pt wire as a counter electrode and Ag/AgCl non aqueous reference electrode. The ferrocene/ferrocenium couple was observed at E^0 (ΔE_p) = 0.2 V (100 mV) under these experimental conditions. ^{1}H (400 MHz) and ^{13}C NMR (100 MHz) spectra of the ligand were recorded on a JEOL RESONANCE ECZ 400S spectrophotometer, using $Si(CH_3)_4$ as internal standard. ESI-MS spectra of the samples were recorded on a JEOL JMS 600 instrument.

2.3 Synthesis of the ligand

***N*⁴,*N*⁵-Bis(4-fluorophenyl)-1*H*-imidazole-4,5-dicarboxamide (LH_3).** To 50 mL of a dichloromethane solution of imidazole-4,5-dicarboxylic acid (156 mg, 1 mmol), oxaloyl chloride (252 mg, 2 mmol) was added and stirred at room temperature for 3 hour in nitrogen atmosphere. The excess of oxaloyl chloride was removed in vacuum. A mixture of 4-fluoroaniline (222 mg, 2 mmol) and triethylamine (303 mg, 3 mmol) was added dropwise at 0 °C under nitrogen atmosphere and the reaction mixture stirred at room temperature for 6 hour. The solution was neutralized by diluted aqueous solution of $NaHCO_3$. The aqueous phase was extracted with dichloromethane (3 × 100 mL). After drying, evaporation of the organic phase produced a white solid. The product was crystallized from dichloromethane. Yield: 73%, elemental anal. calc. for $C_{17}H_{12}N_4O_2F_2$ (in %): C, 59.65; H, 3.53; N, 16.37 found: C, 59.40; H, 3.51; N, 16.30. IR (KBr, cm^{-1}), see Fig. S1 (ESI†): *ν* 3352 (imidazole N–H stretching), 3162 (amide N–H stretching), 2833 (Ar C–H stretching), 1672 (amide C=O), 1622 (amide N–H in-plane deformation), 1562, 1521 1421 (C–N). ESIMS:*m*/*z* 365{M + Na}, see Fig. S2 (ESI†). ^{1}H NMR (DMSO-d_6, 400 MHz) *δ*, see Fig. S3 (ESI†): 13.64 (s, 1H, NH(imidazole)), 13.19 (s, 1H, NH(amide)), 10.65 (s, 1H, NH(amide)), 8.00 (s, 1H, CH(imidazole)), 7.84–7.17 (8H, ArH). ^{13}C NMR (DMSO-d_6, 100 MHz) *δ*, see Fig. S4 (ESI†): 115.7–115.9 (d, $^2J_{C-F}$ = 23 Hz); 116.2–116.4 (d, $^2J_{C-F}$ = 23 Hz); 121.6, 123.9, 129.9, 133.3, 134.5, 135.3, 137.4, 156.4, 157.7, 158.2, 160.1, 160.6, 163.1 (Fig. 1).

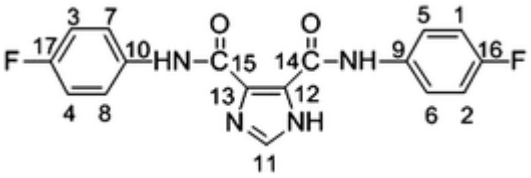

Fig. 1 Molecular sketch of **LH_3**.

2.4 Synthesis of the tetranuclear $Cu_4(LH)_4$ complex

To a 10 mL dichloromethane solution of the ligand LH_2 (0.34 g, 1 mmol), Et_3N (0.202 g, 2 mmol) was added followed by $Cu(ClO_4)_2 \cdot 6H_2O$ (0.37 g, 1 mmol) dissolved in MeOH (50 mL). The reaction mixture was refluxed for 5 hour (the colour of the reaction mixture turned to green within five minutes) leading to the precipitation of a green solid. On cooling, the solid product was filtered off, washed with methanol (2 × 10 mL) and diethyl ether (2 × 10 mL), and finally dried in vacuum. Yield: 67%. Single crystals, suitable for X-ray crystallography, were obtained from a DMF solution. Elemental anal. calc. for $C_{68}H_{40}N_{16}O_8F_8Cu_4$: C, 50.56; H, 2.50; N, 13.87 found: C, 50.63; H, 2.52; N, 13.63%. IR (KBr, cm^{-1}), see Fig. S5 (ESI†): *ν* 2802 (Ar C–H stretching), 1661 (amide C=O), 1580, 1541, 1473. UV/vis (DMF): λ_{max}/nm (ε/M^{-1} cm^{-1}): 308 (36 208), 676 (225).

2.5 Single crystal X-ray crystallography

Single crystals of the complex **$Cu_4(LH)_4$·4DMF** were obtained by slow evaporation of the corresponding DMF solution. A suitable crystal was selected and mounted in fomblin film on a micromount and data were collected on a GV1000 and Atlas diffractometer. The crystal was kept at 120(2) K during data collection. Using Olex2,[44] the structure was solved with the olex2.solve[45] structure solution program employing Charge Flipping and refined with the ShelXL[46] refinement package by means of Least Squares minimisation. The crystal data collection and refinement parameters are given in Table 1.

Table 1 Crystal data and details of the structure determination for **$Cu_4(LH)_4$·4DMF**

Empirical formula	$C_{80}H_{68}N_{20}O_{12}F_8Cu_4$
Formula weight	1907.70
Crystal system	Triclinic
Crystal size/mm^3	0.3267 × 0.1147 × 0.0837
Space group	$P\bar{1}$
a/Å	10.1601(8)
b/Å	12.4693(14)
c/Å	17.1951(11)
α/°	91.449(7)
β/°	98.769(6)
γ/°	113.892(9)
Cell volume, Å^3	1959.3(3)
Z	1
T, K	120(2)
ρ_{calc}, g cm^{-3}	1.617
F_{000}	972.0
μ, mm^{-1}	2.052
Radiation	CuKα (λ = 1.54184)
2Θ range for data collection/°	7.79–149.224
Index ranges	$-12 \le h \le 9$, $-15 \le k \le 15$, $-18 \le l \le 21$
Reflection collected	14 052
Independent reflections	7708 [R_{int} = 0.0261, R_{sigma} = 0.0351]
Data/restraints/parameters	7708/0/563
Goodness-of-fit on F^2	1.028
Final R indexes [$I \ge 2\sigma(I)$]	R_1 = 0.0356, wR_2 = 0.0920
Final R indexes [all data]	R_1 = 0.0433, wR_2 = 0.0972
Largest diff. peak and hole (e Å^{-3})	0.42/−0.53

2.6 Computational details

DFT calculations were performed with the GAUSSIAN09 suite of programs[47] using the hybrid B3LYP exchange–correlation functional.[48] The triple-ζ quality basis set (TZV) proposed by Ahlrichs and co-workers has been used for all atoms, including the metallic centres.[49] A quadratic

convergence method has been employed in the self-consistent-field process in order to improve the obtaining of the correct broken-symmetry states/energies.[50] The approach employed in the determination of the *J* values for polynuclear complexes has been described in detail elsewhere.[42]

3. Results and discussion

3.1 Synthesis

The ligand LH_3 was synthesized following earlier reports for similar compounds.[51,52] Since the acid dichloride formed as intermediate is highly hygroscopic and tend to hydrolyse to the corresponding dicarboxylic acid derivative, the reaction medium should be kept extremely dry. The purity of the obtained product was quite good and no further purification by column chromatography was required. Instead, crystallization from dichloromethane afforded the pure compound. The coordinating efficiency of the deprotonated ligand was clearly observed during the reaction course. Yet, the initial yellow colour of the deprotonated ligand solution changed to green in five minutes after the addition of the Cu(II) salt (Scheme 1). Since the ligand is poorly soluble in methanol, a mixed solvent medium was used for the reaction; thus, the ligand was solubilized in dichloromethane and $Cu(ClO_4)_2$ in methanol. Relative disposition of the amide functionalities in alternated conformation with respect to each other due to internal H-bond formation, makes this ligand as a well-suited bridging system to get polynuclear structures. Although the ligand has three acidic protons, in order to favour a [2 × 2] grid, two equivalent of base were deliberately used to abstract the imidazolic and one of the amidic protons (Scheme 2), thus neutralizing the charge of a single metallic ion. This approach successfully led to the formation of a [2 × 2] square grid of Cu(II) ions.

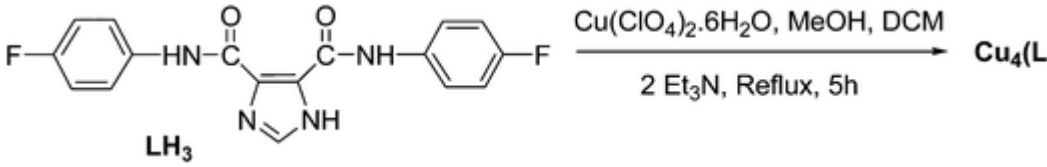

Scheme 1 General reaction scheme for the synthesis of the tetranuclear copper complex **$Cu_4(LH)_4$**.

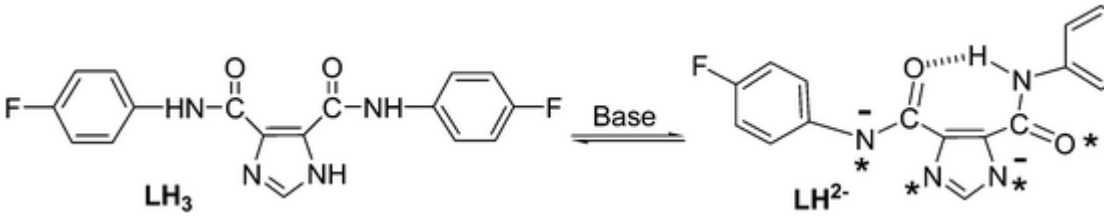

Scheme 2 Deprotonation of the acidic protons. Coordinating atoms are marked with asterisk.

Different techniques, described below, have been employed to totally characterize the tetranuclear, Cu4 complex. Additionally, a thermogravimetric analysis has also been done, see Fig. S6 (ESI†), for the desolvated **$Cu_4(LH)_4$** species.

3.2 Single crystal X-ray structure of $Cu_4(LH)_4$

A green-coloured single crystal of the tetranuclear **$Cu_4(LH)_4$** copper complex was obtained from slow evaporation of a dimethylformamide solution of **$Cu_4(LH)_4$**. The molecular structure of the

complex has been determined by single crystal X-ray diffraction (shown in Fig. 2). Bond lengths and angles around the metal centres are presented in Table S1 (ESI†).

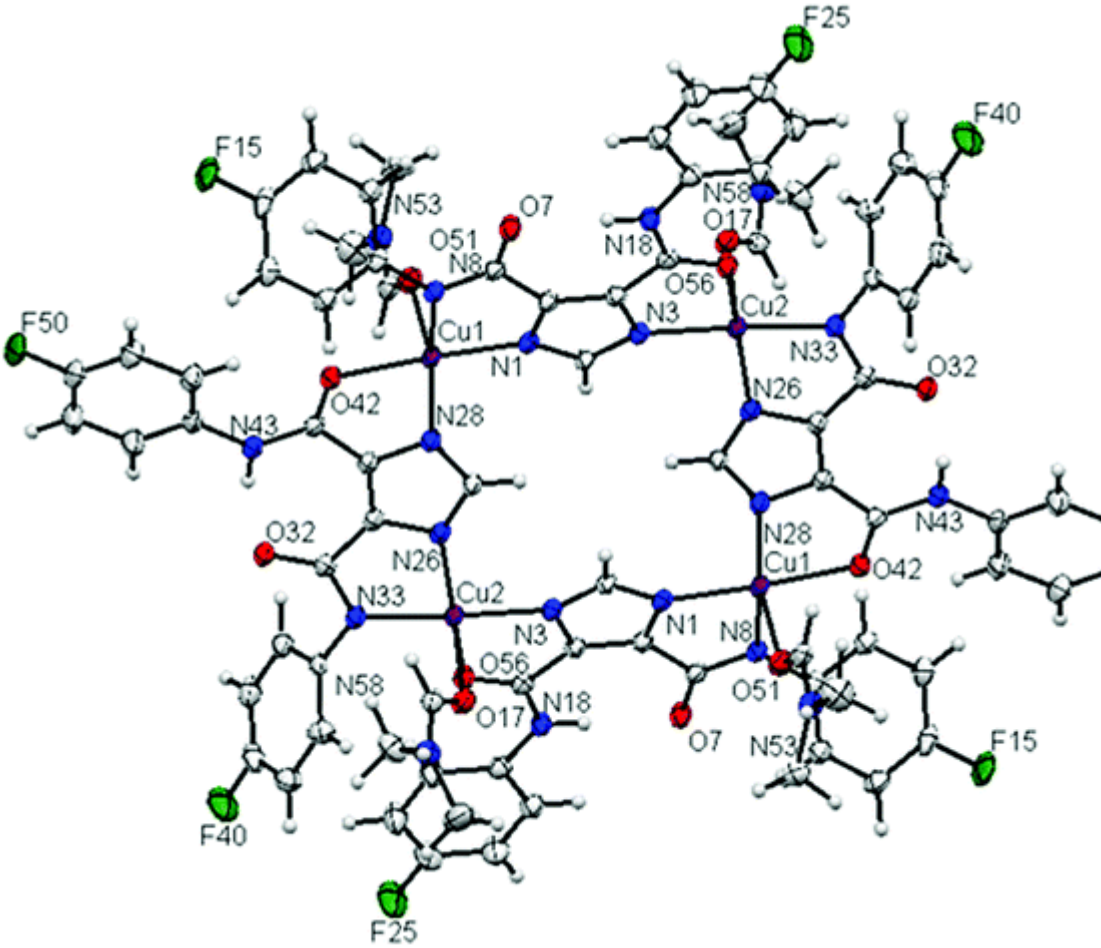

Fig. 2 The ORTEP diagram of the tetranuclear, C_i symmetry, Cu complex **$Cu_4(LH)_4$·4DMF**.

The tetranuclear complex crystallizes in the triclinic system ($P\bar{1}$ space group) with four DMF molecules. Therefore, the molecular formula of the crystal is **$Cu_4(LH)_4$·4DMF**. Single crystal X-ray crystallography shows that each copper centre has a [4 + 1] coordination. The actual geometry around each metal centre was confirmed from the trigonality index (τ).[53] For a five coordination system this is given by the relation $\tau = (\beta - \alpha)/60$, where β and α are the two largest bond angles of the coordination centre, τ being 0 for a perfect square-pyramidal geometry and 1 for a perfect trigonal-bipyramidal geometry. In our **$Cu_4(LH)_4$·4DMF** complex, the two different Cu1 and Cu2 centres presented the structural indices τ 0.047 and 0.14, respectively, evidencing just small deviations from the square-pyramidal geometry.

The basal plane of the pyramid is formed by a neutral imidazolic nitrogen atom and a deprotonated amidic nitrogen atom belonging to one ligand along with the deprotonated imidazolic nitrogen atom and a neutral amidic oxygen atom belonging to another ligand. Thus, a N_3O set of donor atoms completes the square, basal plane of the square pyramid scaffold. The

fifth, apical position in the pyramid is completed by a dimethylformamide molecule coordinated through its oxygen atom. Note that the two amide functionalities of each ligand coordinates differently with Cu(II) ions: one of the amide coordinates through the nitrogen atom (Cu1) and the other through the oxygen atom (Cu2). The alternated arrangement of the amide groups with respect to the pivotal imidazole ring is probably induced by the intramolecular H-bond (per ligand) that is formed between the non-coordinated oxygen atom of one amide group and the NH of the other one (Fig. 1), thus resulting in two copper atoms positioned on the same side of the ligand, favouring the square shape among other possible supramolecular spatial arrangements.

Cu–N distances are found to range from 1.974 to 2.000 Å, whereas Cu–O distances for equatorial and axial positions range from 2.029 to 2.060 Å and 2.213 to 2.254 Å respectively (Table S1, ESI†). *cis*-Position angles in the basal plane around Cu1 fall in the range 80.80(7) to 98.51(6)°; similar values were found for Cu2 with values ranging 81.33(7) to 107.34(7)°. On the other hand, *trans*-position angles around Cu1 are 163.44(8) and 176.66(7)°, whereas for Cu2 these values are 160.09(7) and 171.96(8)°. All these numbers clearly indicate a greater deviation of the Cu2 centre from the square-pyramidal geometry, which is also reflected by the corresponding τ values (*vide supra*). The square spatial arrangement is then also supported by the formation of four strong intramolecular NH···O and four weak intramolecular CH···O hydrogen bonds (Table 2).

Table 2 Geometrical features (Å and °) of hydrogen bonds[a]

Donor (D)–H···acceptor (A)	***d*(D–H)**	***d*(H–A)**	***d*(D–A)**	**D–H–A**
Strong				
N(18)–H(18)···O(7)	0.88	1.97	2.810(2)	159.8
N(43)–H(43)···O(32)	0.88	1.91	2.769(3)	164.2
Weak				
C(24)–H(24)···O(17)	0.95	2.21	2.829(3)	122.3
C(45)–H(45)···O(42)	0.95	2.26	2.862(3)	120.8

a **Owing the C_i symmetry of the tetranuclear unit, each entry is established twice on each tetranuclear $Cu_4(LH)_4 \cdot 4DMF$ unit in the crystal structure.**

Interestingly, the coordinated DMF molecules form layers in between interpenetrated units of alternate up (the corresponding DMF molecule in apical position presents a relative up disposition) and down (the DMF molecule has a relative down disposition) tetranuclear species that are sandwiched, with intermolecular Cu1···Cu1 (or Cu2···Cu2) distances of just 4.187 Å, whereas the corresponding crossed intermolecular Cu1···Cu2 distances are 7.489 Å. Traversing each DMF layer, the shorter interlayer Cu1···Cu1 distances are 8.785 Å, and the corresponding crossed Cu1···Cu2 distances are 8.962 Å (Fig. 3).

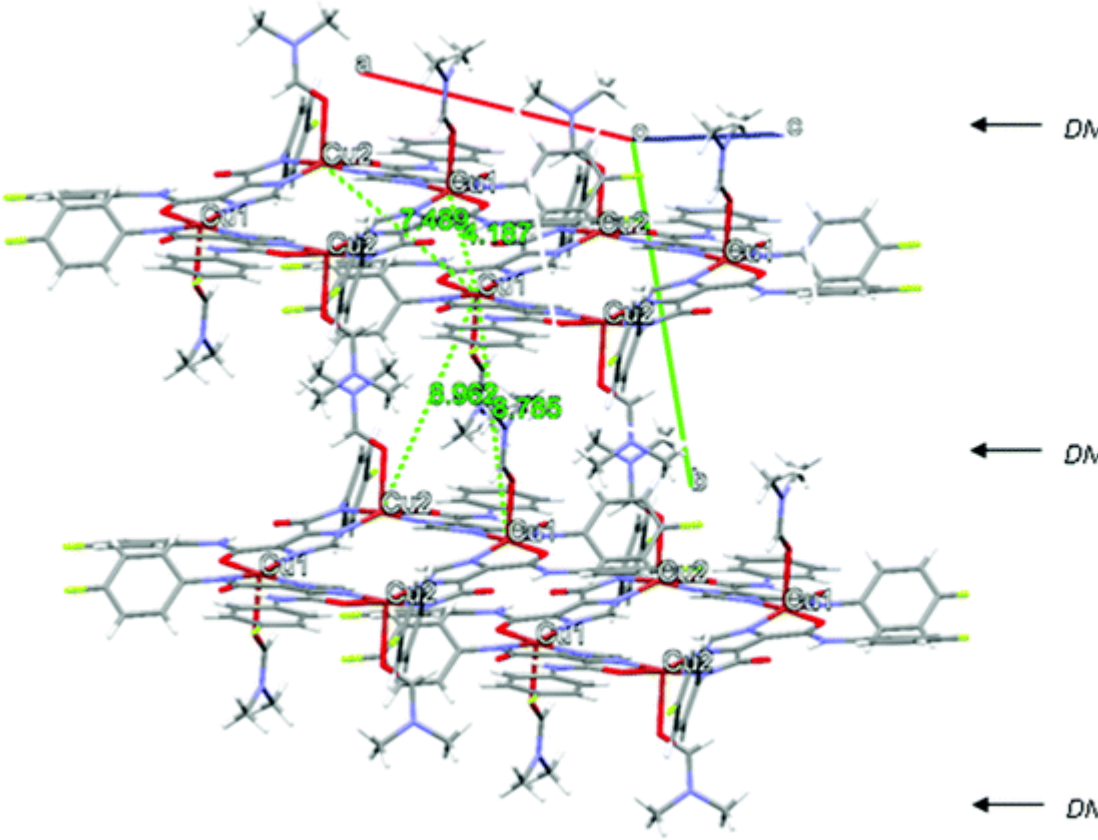

Fig. 3 DMF layers created by alternating interpenetrated up/down tetranuclear **$Cu_4(LH)_4$** units.

3.3 Electronic spectra

The UV-vis spectrum of the ligand LH_3 was recorded in dimethylformamide in the range 260–600 nm, whereas for the copper complex the spectrum was recorded in the same solvent up to 1200 nm in the NIR region. The only relevant peaks appeared in the ligand at 289 nm and in the metal complex at 308 nm, having both almost similar spectral features and being then assigned to an intraligand transition in the case of the complex. In the visible region the complex shows a weak band at 676 nm (Fig. 4) due to a d–d transition.[54–56]

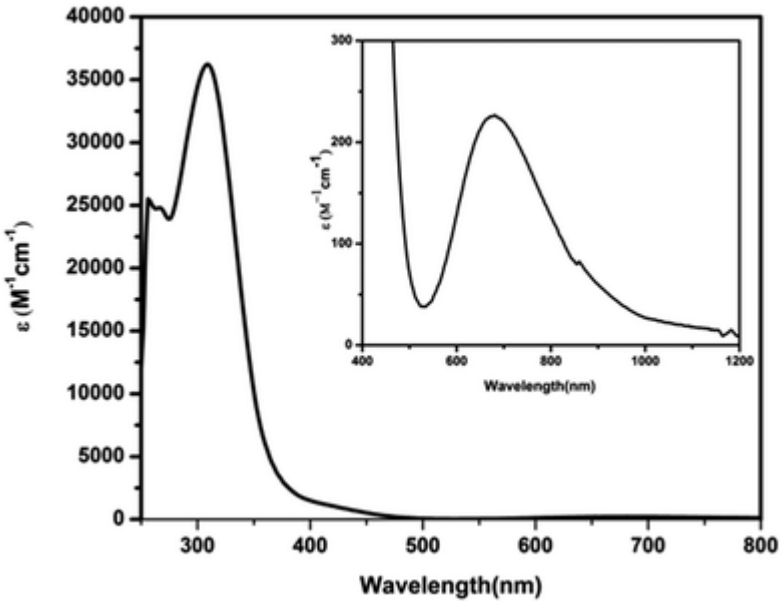

Fig. 4 Electronic spectrum of **$Cu_4(LH)_4$** in DMF.

3.4 Catalytic activity

Catechol oxidase catalyzes completely the oxidation of catechols (*i.e. o*-diphenols) to the corresponding quinones, and this process is known as catecholase activity[57,58] (Fig. 5).

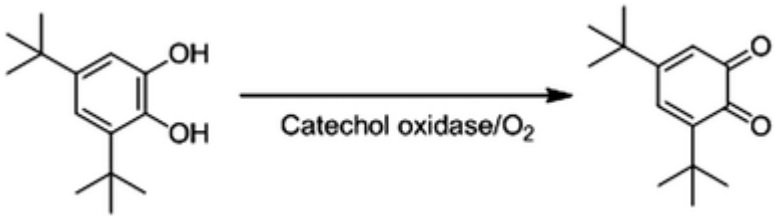

Fig. 5 Catecholase activity.

For the catecholase activity 3,5-di-*tert*-butylcatechol (3,5-DTBC) is the most widely used substrate due to its low redox potential for the quinone–catechol couple, which makes it easily oxidized to the corresponding quinone, 3,5-di-*tert*-butylquinone (3,5-DTBQ). Its bulky substituents make further oxidation reactions (*e.g.*, ring opening) slower. The detection of the oxidation of 3,5-DTBC to the corresponding 3,5-DTBQ can be followed by the development of the absorption band at about 400 nm. Therefore, activities and reaction rates can be determined using electronic spectroscopy by following the appearance of the characteristic absorption of the 3,5-di-*tert*-butyl-*o*-quinone (3,5-DTBQ). For this purpose a 1×10^{-5} M solution of complex was treated with 300 equivalents of 3,5-DTBC under aerobic condition in DMF solution[59,60] due to the good solubility of the complex and the substrate. After addition of 3,5-DTBC, the increase of the absorption at 400 nm, which is indicative of an oxidation to the corresponding quinone (3,5-DTBQ), indicates catecholase activity (Fig. 6).

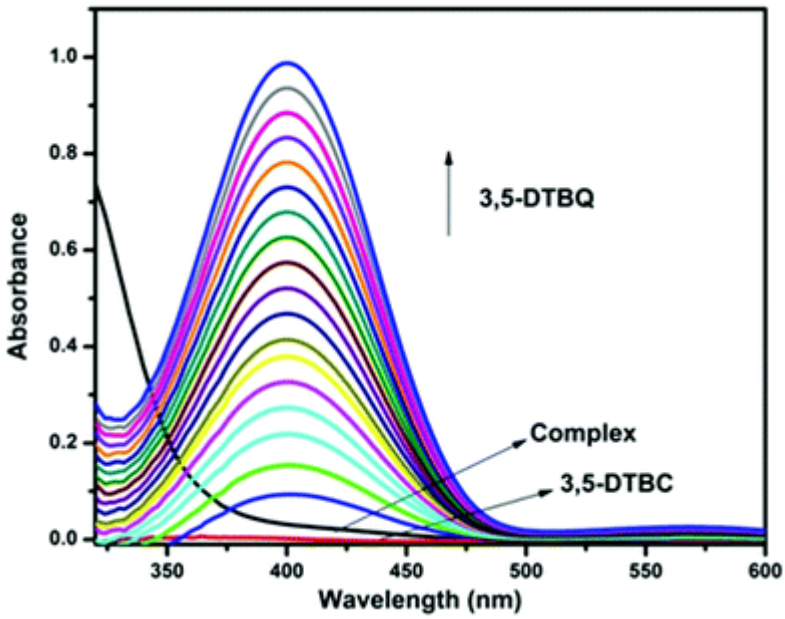

Fig. 6 Increase in the absorbance after the addition of 300 equivalents of 3,5-DTBC to a solution of **$Cu_4(LH$** The spectra were recorded every 10 minutes.

To determine the dependence of the rates on the substrate concentration and various kinetic parameters, 1×10^{-5} M solutions of the complex were prepared with increasing concentrations of 3,5-DTBC (from 20 to 100 eq.) under aerobic conditions. First-order dependence was observed at low concentrations of the substrate, whereas saturation kinetics was found at higher concentrations of the substrate (Fig. S7a, ESI†). The dependence on the substrate concentration indicates that a catalyst–substrate binding is the initial step in the catalytic mechanism. A treatment on the basis of Michaelis–Menten approach was, therefore, applied and linearized by means of Lineweaver–Burk plot (Fig. S7b, ESI†) to calculate various kinetic parameters such as Michaelis–Menten constant ($K_m = 1.61 \times 10^{-2}$ M), maximum initial rate ($V_{max} = 2.174 \times 10^{-4}$ M h^{-1}) and turn-over number of the complex ($k_{cat} = 21.74$ h^{-1}, calculated by dividing the V_{max} value by the complex concentration).

Several factors, *e.g.* Cu···Cu distance, coordination geometry around the metal center, nature of the exogenous bridging ligand, flexibility of the primary ligand, *etc.* influence the catalytic rate. A Cu ···Cu distance in the range of 2.9–3.25 Å has been proposed for the best catalytic activity. In the crystal structure of the *met* form of the enzyme, two trigonal pyramidal copper(II) centers are bridged by a hydroxo group. But in model systems a better activity for trigonal bipyramidal,[37] square pyramidal[38] or square planar[51] Cu(II) centers were reported, *i.e.*, the activity can be observed both for four or five coordinate Cu(II) centers. In the present **$Cu_4(LH)_4$·4DMF** molecule, all the four Cu(II) centers have nearly square pyramidal

geometry. Cu···Cu distances (sides: 6.167 and 6.174 Å; diagonal: 8.813 Å) are quite long which may be the reason for lower catalytic activity. Moreover the rigidity of the bridging ligand may also influence the activity.

3.5 Electrochemical properties

The electrochemical behaviour of the ligand and complex has been investigated by cyclic voltammetry in DMF solution. Cyclic voltammogram of the Cu(II) complex exhibits one irreversible reduction of Cu(II) to Cu(I) (E_{pc}) at −0.289 V/(Ag/AgCl) and one ligand-based reversible reduction at −1.21 V/(Ag/AgCl), see Fig. S8 (ESI†).

3.6 Magnetic properties and DFT calculations

The magnetic properties of the **$Cu_4(LH)_4$** complex in form of χT *vs.* T (in blue) and χ *vs.* T (in red) are depicted in Fig. 7. At 300 K, the χT amounts to 1, that is below the expected value for four non interacting S = 1/2 copper atoms (χT = 1.5 with g = 2.0). TheχT value decreases to 0.2 on cooling to 10 K and remains almost constant until 2 K. On lowering the temperature from 300 K, the χ *vs.* T curve presents a maximum at 170 K. All these facts indicate that a global antiferromagnetic (AF) coupling occurs in the sample. The increase at low temperature for χ reveals the presence of some monomeric impurities.

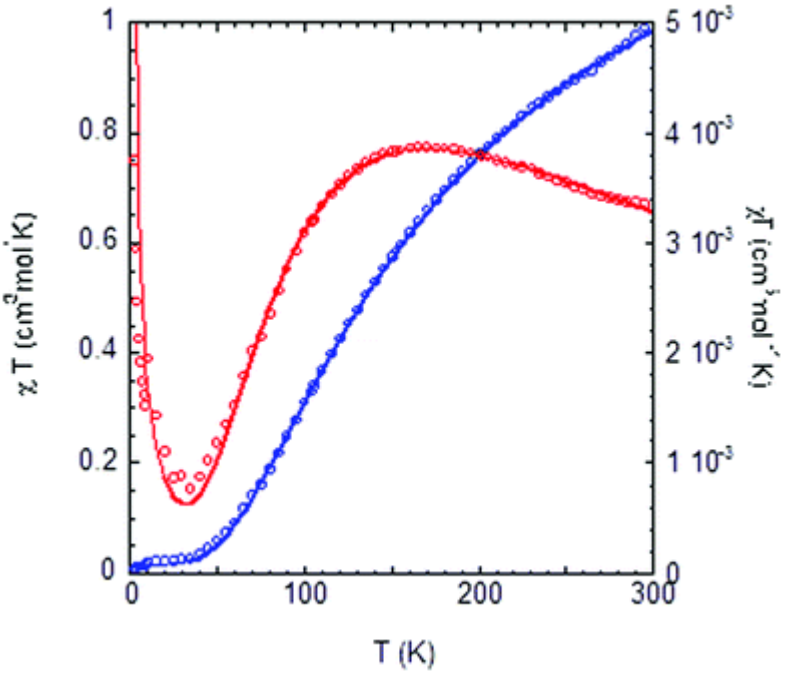

Fig. 7 Temperature dependence of χ (○ (red), experimental data; ⎯ (red), best fit) and χT (○ (blue), experim for the crystalline sample of **$Cu_4(LH)_4$·4DMF**.

Due to the C_i symmetry of the **$Cu_4(LH)_4$** unit, two different Cu–Cu distances are present in the Cu_4 square. Therefore, two main different magnetic pathways could be considered (ignoring the diagonals that actually are expected to be negligible). Consequently, the whole exchange coupling could be described by the following spin Hamiltonian:

$$\mathbf{H} = -J_1\left(\hat{S}_{Cu1}\cdot\hat{S}_{Cu2} + \hat{S}_{Cu3}\cdot\hat{S}_{Cu4}\right) - J_2\left(\hat{S}_{Cu2}\cdot\hat{S}_{Cu3} + \hat{S}_{Cu4}\cdot\hat{S}_{Cu1}\right)$$

The experimental data were simulated using a least-squares fitting program with a full-matrix diagonalization of the exchange coupling. Best fits (solid lines in Fig. 7) were obtained for J_1 = −143.4 cm^{-1}, J_2 = −169.0 cm^{-1}, g = 2.017 and ρ = 0.043, where ρ is the amount of monomeric impurity ($R_{\chi T} = 6.21 \times 10^{-5}$ with $R_{\chi T} = [\Sigma(\chi T_{calc} - \chi T_{obs})^2/\Sigma(\chi T_{obs})^2]$).

Numerous factors have been proposed to correlate the magnitude of the coupling exchange and the structure of dinuclear compounds containing the imidazolate bridge.[62] The more relevant seems to be the influence of the Cu–N–N angle, α,[63] that was shown by Massoud *et al.* to correlate linearly with $-J$.[64] Using this correlation for the **Cu$_4$(LH)$_4$** complex under study, where the average of all the Cu–N–N angles is 175.57°, J should be about −187.5 cm^{-1}, which is a slightly higher value than the experimental result (*vide supra*). Nevertheless, other parameters were identified as influencing the coupling exchange[62c] on these type of complexes, such as the dihedral angle between the plane of the magnetic orbitals of the Cu^{II} ions, the plane of the imidazolate bridge or the increase of the AF (antiferromagnetic) coupling with the increase of the Cu–N–C angle.[65]

DFT calculations performed on a unit of the tetranuclear **Cu$_4$(LH)$_4$·4DMF** complex as found in the crystal structure furnished the following values for the magnetic coupling constants, as shown in Fig. 8: J_1 = −78.3, J_2 = −97.6, J_3 = −1.42 and J_4 = +0.536 cm^{-1}. These values could be obtained by calculating five broken-symmetry spin states (without spin projection), namely a quintuplet (++++), a triplet (−+++) and three different singlets [(++−−), (+−+−), (+−−+)]. Magnetic coupling constants J_3 and J_4correspond to both diagonals in the square defined by the four metallic centres (Fig. 8). As expected, the later values are small enough (compared to J_1 and J_2) to be negligible on the corresponding spin Hamiltonian of the experimental equation and this justifies the used Hamiltonian based just on J_1 and J_2. Therefore, the calculated theoretical values agree well with the experimental found values, showing a moderately strong antiferromagnetic (AF) coupling between the copper(II) ions. This behaviour could be due to a fairly good orbital overlap between the magnetic orbitals of the metallic centres and the corresponding orbitals of some ligand atoms (superexchange mechanism), and also probably to the absence of mechanisms favouring a ferromagnetic (F) coupling.[66]

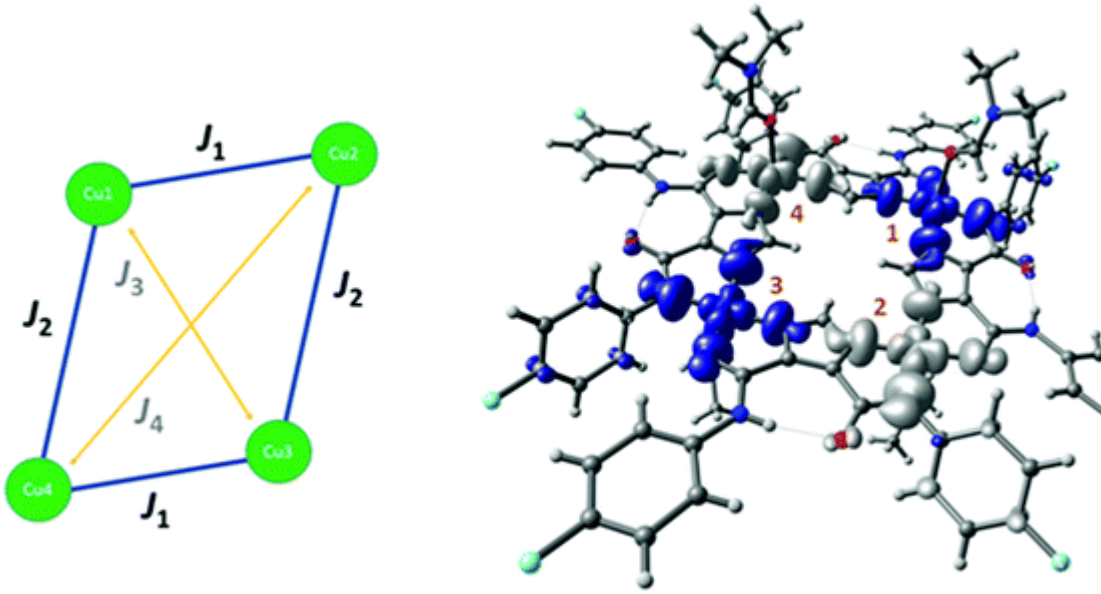

Fig. 8 (a) Schematic representation of the **$Cu_4(LH)_4$·4DMF** complex showing the considered magnetic path its C_i symmetry. (b) Spin density isosurface showing the negative (blue) and positive (grey) isodensity value lowest-energy broken-symmetry singlet state.

The spin density map displayed for the most stable magnetic state (the singlet with alternating +−+− spin signs, see Fig. 8) clearly reveals an AF coupling through a delocalized σ exchange mechanism (from the $d_{x^2-y^2}$ copper(II) orbitals to the sp^2 ones of the imidazole N atoms directly attached to them) with the most part of the spin density concentrated on the copper(II) ions (as they are the magnetic centres) and the neighbour donor atoms. A close inspection on the spin density values shows that the magnetic pathway mainly goes through the imidazolyl moiety following an inner (N–C–N) pathway. Therefore, it could be pointed out that the magnetic interaction pathways are mainly placed, as expected, in the molecular plane. Some selected spin densities (in electrons) for this broken-symmetry singlet state are presented in Table S2 (ESI†). Despite the good qualitative agreement in sign and magnitude order between the experimental and theoretical coupling values, the later are about half of the experimental ones as reported for other copper polynuclear complexes.[67] This may be due to either intrinsic limitations of the approach used in the calculation of the *J* values for copper atoms or to a high flexibility of the copper complex[68] that leads to significant geometric differences between high and low temperature conformations, which is crucial in the experimental determination but that DFT calculations cannot take into account.

4. Conclusions

In this work a new bis-amide ligand suitable for metal coordination has been reported. This ligand successfully generated a $C_i$symmetry, [2 × 2] grid, square copper complex. During complexation with copper(II) perchlorate, both amide groups behave differently towards the metal, probably due to the formation of a strong intramolecular NH···O H-bond per ligand. One amide functionality coordinates through deprotonated amide nitrogen whereas the other one uses the oxygen atom in neutral form. The complex crystallises along interpenetrated Cu_4 units separated by layers of interwoven DMF molecules, which in turn are coordinated to the copper(II) ions in apical positions following an up/down pattern. The title complex shows mild catecholase activity with a k_{cat} value of 21.74 h^{-1}. The tetranuclear copper complex showed an antiferromagnetic interaction as observed from the lower value of χT and the pattern of χ *vs.* T plot. Magnetic coupling constants calculated theoretically corroborate the experimental findings, showing a good qualitative agreement in sign and magnitude. The antiferromagnetic behaviour of the complex may be nicely interpreted in terms of a super exchange mechanism due to a strong overlap between the magnetic orbital of the metallic centres and the ligands ones, and also probably owing to the absence of mechanisms leading to ferromagnetic coupling. Polynuclear copper complexes play important role in biological oxidation catalysis. The type of molecule reported in the present study shows mild catecholase activity. A systematic variation in the substitutions on ligand to control the electronic as well as the magnetic properties may enlight the underlying mechanism. Therefore further improvement of the present system will be perused in future accordingly.

Acknowledgements

S. N. thanks CSIR, New Delhi, Govt. of India for funding this work through CSIR Project (No. 01(2577)/12/EMR-II, 03/04/2013). S. N. is grateful to AICTE, New Delhi, Govt. of India for sanctioning a UV-vis-NIR spectrophotometer through AICTE-RPS Project (No. 8023/RID/RPS-10/Pvt (II Policy)/2011–12). SN also acknowledges the NMR spectral facility established in the Chemistry Dept. BITMesra through the DST FIST Program (SR/FST/CSI-242/2012).The authors thank CIF, BIT-Mesra, Ranchi, India for analytical measurements. A. P. thanks UGC, New Delhi, India for MANF-JRF fellowship. We also thank the *Centro de Supercomputación de la Universidad de Granada* (CSIRC) for computational facilities.

References

1. W. Lucas, *Viral Capsids and Envelopes: Structure and Function*, John Wiley & Sons, New York, 2001 Search PubMed.
2. A. J. Olson, Y. H. Hu and E. Keinan, *Proc. Natl. Acad. Sci. U. S. A.*, 2007, **104**, 20731–20736 CrossRef CAS PubMed.
3. J. T. Davis and G. P. Spada, *Chem. Soc. Rev.*, 2007, **36**, 296–313 RSC.
4. J. T. Davis, *Angew. Chem., Int. Ed.*, 2004, **43**, 668–698 CrossRef CAS PubMed.
5. J. R. Nitschke, *Acc. Chem. Res.*, 2007, **40**, 103–112 CrossRef CAS PubMed.
6. L. K. Thompson, *Coord. Chem. Rev.*, 2002, **233**, 193–206 CrossRef.
7. M. M. Smulders, I. A. Riddell, C. Browne and J. R. Nitschke, *Chem. Soc. Rev.*, 2013, **42**, 1728–1754 RSC.

8. B. Champin, P. Mobian and J. P. Sauvage, *Chem. Soc. Rev.*, 2007, **36**, 358–366 RSC.
9. Y. E. Alexeev, B. I. Kharisov, T. C. H. Garcia and A. D. Garnovskii, *Coord. Chem. Rev.*, 2010, **254**, 794–831 CrossRef CAS.
10. R. Chakrabarty, P. S. Mukherjee and P. J. Stang, *Chem. Rev.*, 2011, **111**, 6810–6918 CrossRef CAS PubMed.
11. M. Ruben, J. Rojo, F. J. Romero-Salguero, L. H. Uppadine and J.-M. Lehn, *Angew. Chem., Int. Ed.*, 2004, **43**, 3644 CrossRef CAS PubMed.
12. L. K. Thompson, O. Waldmann and Z. Xu, *Coord. Chem. Rev.*, 2005, **249**, 2677 CrossRef CAS.
13. John G. Hardy, *Chem. Soc. Rev.*, 2013, **42**, 7881–7899 RSC.
14. W. B. Lin, W. J. Rieter and K. M. L. Taylor, *Angew. Chem., Int. Ed.*, 2009, **48**, 650–658 CrossRef CAS PubMed.
15. K. L. Wang, I. Ovchinnikov, F. X. Xiu, A. Khitun and M. Bao, *J. Nanosci. Nanotechnol.*, 2011, **11**, 306–313 CrossRef CAS PubMed.
16. S. K. Dey, L. K. Thompson and L. N. Dawe, *Chem. Commun.*, 2006, 4967–4969 RSC.
17. D. L. Caulder, C. Bruckner, R. E. Powers, S. Konig, T. N. Parac, J. A. Leary and K. N. Raymond, *J. Am. Chem. Soc.*, 2001, **123**, 8923–8938 CrossRef CAS PubMed.
18. H. Sigel and R. B. Martin, *Chem. Rev.*, 1982, **82**, 385–426 CrossRef CAS.
19. D. S. Marlin and P. K. Mascharak, *Chem. Soc. Rev.*, 2000, 69–74 RSC.
20. J. W. Peters, M. H. Stowell, M. Soltis, M. G. Finnegan, M. K. Johnson and D. C. Rees, *Biochemistry*, 1997, **36**, 1181–1187 CrossRef CAS PubMed.
21. G. D. Pirngruber, L. Frunz and M. Luchinger, *Phys. Chem. Chem. Phys.*, 2009, **11**, 2928–2938 RSC.
22. H. R. Khavasi, K. Sasan, M. Pirouzmand and S. N. Ebrahimi, *Inorg. Chem.*, 2009, **48**, 5593–5595 CrossRef CAS PubMed.
23. A. P. Singh, A. Ali and R. Gupta, *Dalton Trans.*, 2010, **39**, 8135–8138 RSC.
24. A. Mishra, A. Ali, S. Upreti, M. S. Whittingham and R. Gupta, *Inorg. Chem.*, 2009, **48**, 5234–5243 CrossRef CAS PubMed.
25. P. Srinivas, P. R. Likhar, H. Maheswaran, B. Sridhar, K. Ravikumar and M. LakshmiKantam, *Chem. – Eur. J.*, 2009, **15**, 1578–1581 CrossRef CAS PubMed.
26. B. M. Trost and I. Hachiya, *J. Am. Chem. Soc.*, 1998, **120**, 1104–1105 CrossRef CAS.
27. D. A. Conlon and N. Yasuda, *Adv. Synth. Catal.*, 2001, **343**, 137–138 CrossRef CAS.
28. E. I. Solomon, U. M. Sundaramand and T. E. Machonkin, *Chem. Rev.*, 1996, **96**, 2563–2606 CrossRef CAS PubMed.
29. I. A. Koval, P. G. Amez, C. Belle and K. Reedijk, *Chem. Soc. Rev.*, 2006, **35**, 814–840 RSC.
30. T. Klabunde, C. Eicken, J. C. Sacchettini and B. Krebs, *Nat. Struct. Biol.*, 1998, **5**, 1084–1090 CrossRef CAS PubMed.
31. A. Banerjee, R. Singh, E. Colacio and K. K. Rajak, *Eur. J. Inorg. Chem.*, 2009, 277–284 CrossRef CAS.
32. L. Gasque, V. M. Ugalde-Saldivar, I. Membrillo, J. Olguin, E. Mijangos, S. Bernes and I. Gonzalez, *J. Inorg. Biochem.*, 2008,**102**, 1227–1235 CrossRef CAS PubMed.
33. A. Banerjee, S. Sarkar, D. Chopra, E. Colacio and K. K. Rajak, *Inorg. Chem.*, 2008, **47**, 4023–4031 CrossRef CAS PubMed.

34. M. Merkel, N. Moeller, M. Piacenza, S. Grimme, A. Rompel and B. Krebs, *Chem. – Eur. J.*, 2005, **11**, 1201–1209 CrossRef CAS PubMed.
35. I. A. Koval, C. Belle, K. Selmeczi, C. Philouze, E. Saint-Aman, A. M. Schuitema, P. Gamez, J.-L. Pierre and J. Reedijk, *J. Biol. Inorg. Chem.*, 2005, **10**, 739–750 CrossRef CAS PubMed.
36. I. A. Koval, D. Pursche, A. F. Stassen, P. Gamez, B. Krebs and J. Reedijk, *Eur. J. Inorg. Chem.*, 2003, 1669–1674 CrossRef CAS.
37. C. Belle, C. Beguin, I. Gautier-Luneau, S. Hamman, C. Philouze, J. L. Pierre, F. Thomas, S. Torelli, E. Saint-Aman and M. Bonin, *Inorg. Chem.*, 2002, **41**, 479–491 CrossRef CAS PubMed.
38. J. Reim and B. Krebs, *J. Chem. Soc., Dalton Trans.*, 1997, 3793–3804 RSC.
39. A. Biswas, L. K. Das, M. G. B. Drew, C. Diaz and A. Ghosh, *Inorg. Chem.*, 2012, **51**, 10111–10121 CrossRef CAS PubMed.
40. R. Sanyal, P. Kundu, E. Rychagova, G. Zhigulin, S. Ketkov, B. Ghosh, S. K. Chattopadhyay, E. Zangrando and D. Das, *New J. Chem.*, 2016, **40**, 6623–6635 RSC.
41. S. Majumder, S. Sarkar, S. Sasmal, E. C. Sanudo and S. Mohanta, *Inorg. Chem.*, 2011, **50**, 7540–7554 CrossRef CAS PubMed.
42. (*a*) E. Ruiz, J. Cano, S. Alvarez and P. Alemany, *J. Comput. Chem.*, 1999, **20**, 1391–1400 CrossRef CAS; (*b*) E. Ruiz, S. Alvarez, A. Rodríguez-Fortea, P. Alemany, Y. Puoillon and C. Massobrio, in *Magnetism: Molecules to Materials*, ed. J. S. Miller and M. Drillon, Wiley-VCH, Weinheim, 2001, vol. II, p. 5572 Search PubMed; (*c*) E. Ruiz, A. Rodríguez-Fortea, J. Cano, S. Alvarez and P. Alemany, *J. Comput. Chem.*, 2003, **24**, 982–989 CrossRef CAS PubMed; (*d*) E. Ruiz, S. Alvarez, J. Cano and V. Polo, *J. Chem. Phys.*, 2005, **123**, 164110 CrossRef PubMed.
43. D. T. Sawyer, A. Sobkowiak and J. L. Roberts Jr., *Electrochemistry for Chemists*, John Wiley and Sons, New York, 2nd edn, 1995. p. 333 Search PubMed.
44. O. V. Dolomanov, L. J. Bourhis, R. J. Gildea, J. Howard and H. Puschmann, *J. Appl. Crystallogr.*, 2009, **42**, 339–341 CrossRef CAS.
45. L. J. Bourhis, O. V. Dolomanov, R. J. Gildea, J. Howard and H. Puschmann, *Acta Crystallogr., Sect. A: Found. Adv.*, 2015, **71**, 59–75 CrossRef CAS PubMed.
46. G. M. Sheldrick, *Acta Crystallogr.*, 2008, **64**, 112–122 CrossRef CAS PubMed.
47. M. J. Frisch, G. W. Trucks, H. B. Schlegel, G. E. Scuseria, M. A. Robb, J. R. Cheeseman, G. Scalmani, V. Barone, B. Mennucci, G. A. Petersson, H. Nakatsuji, M. Caricato, X. Li, H. P. Hratchian, A. F. Izmaylov, J. Bloino, G. Zheng, J. L. Sonnenberg, M. Hada, M. Ehara, K. Toyota, R. Fukuda, J. Hasegawa, M. Ishida, T. Nakajima, Y. Honda, O. Kitao, H. Nakai, T. Vreven, J. A. Montgomery Jr, J. E. Peralta, F. Ogliaro, M. Bearpark, J. J. Heyd, E. Brothers, K. N. Kudin, V. N. Staroverov, T. Keith, R. Kobayashi, J. Normand, K. Raghavachari, A. Rendell, J. C. Burant, S. S. Iyengar, J. Tomasi, M. Cossi, N. Rega, N. J. Millam, M. Klene, J. E. Knox, J. B. Cross, V. Bakken, C. Adamo, J. Jaramillo, R. Gomperts, R. E. Stratmann, O. Yazyev, A. J. Austin, R. Cammi, C. Pomelli, J. W. Ochterski, R. L. Martin, K. Morokuma, V. G. Zakrzewski, G. A. Voth, P. Salvador, J. J. Dannenberg, S. Dapprich, A. D. Daniels, Ö. Farkas, J. B. Foresman, J. V. Ortiz, J. Cioslowski and D. J. Fox, *Gaussian 09, Revision B.01*, Gaussian, Inc., Wallingford CT, 2010 Search PubMed.
48. (*a*) A. D. Becke, *Phys. Rev. A: At., Mol., Opt. Phys.*, 1988, **38**, 3098–3100 CrossRef CAS; (*b*) C. Lee, W. Yang and R. G. Parr,*Phys. Rev. B: Condens.*

Matter Mater. Phys., 1988, **37**, 785–789 CrossRef CAS; (*c*) A. D. Becke, *J. Chem. Phys.*, 1993, **98**, 5648–5652 CrossRef CAS.
49. A. Schäfer, C. Huber and R. Ahlrichs, *J. Chem. Phys.*, 1994, **100**, 5829–5835 CrossRef.
50. G. B. Bacskay, *Chem. Phys.*, 1981, **61**, 385–404 CrossRef CAS.
51. M. N. Bhattacharjee, M. K. Chaudhuri and D. T. Khathing, *J. Chem. Soc., Dalton Trans.*, 1982, 669–670 RSC.
52. S. Hazra, S. Naskar, D. Mishra, S. I. Gorelsky, H. M. Figgie, W. S. Sheldrick and S. K. Chattopadhyay, *Dalton Trans.*, 2007, 4143–4148 RSC.
53. A. W. Addison, T. N. Rao, J. Reedijk, J. Van Rijn and G. C. Verschoor, *J. Chem. Soc., Dalton Trans.*, 1984, 1349–1356 RSC.
54. R. H. Holm, G. W. Everett Jr. and A. Chakravorty, *Prog. Inorg. Chem.*, 1966, **7**, 83–214 CAS.
55. A. Biswas, M. G. B. Drew, C. J. Gomez-Garcıa and A. Ghosh, *Inorg. Chem.*, 2010, **49**, 8155–8163 CrossRef CAS PubMed.
56. A. Parween, T. K. Mandal, R. Guillot and S. Naskar, *Polyhedron*, 2015, **99**, 34–46 CrossRef CAS.
57. P. Kar, R. Haldar, C. J. Gómez-García and A. Ghosh, *Inorg. Chem.*, 2012, **51**, 4265–4273 CrossRef CAS PubMed.
58. S. Kr Dey and A. Mukherjee, *New J. Chem.*, 2014, **38**, 4985–4995 RSC.
59. J. Kaizer, G. Barath, R. Csonka, G. Speier, L. Korecz, A. Rockenbauer and L. Parkanyi, *J. Inorg. Biochem.*, 2008, **102**, 773–780 CrossRef CAS PubMed.
60. N. C. Jana, P. Brandão and A. Panja, *J. Inorg. Biochem.*, 2016, **159**, 96–106 CrossRef CAS PubMed.
61. (*a*) D. Ghosh, T. K. Lal, S. Ghosh and R. Mukherjee, *J. Chem. Soc., Chem. Commun.*, 1996, 13–14 RSC; (*b*) D. Ghosh and R. Mukherjee, *Inorg. Chem.*, 1998, **37**, 6597–6605 CrossRef CAS PubMed.
62. (*a*) G. Kolks, S. J. Lippard, J. V. Waszczak and H. R. Lilienthal, *J. Am. Chem. Soc.*, 1982, **104**, 717–725 CrossRef CAS; (*b*) C. Benelli, R. K. Bunting, D. Gatteschi and C. Zanchini, *Inorg. Chem.*, 1984, **23**, 3074–3076 CrossRef CAS; (*c*) A. Bencini, C. Benelli, D. Gatteschi and C. Zanchini, *Inorg. Chem.*, 1986, **25**, 398–400 CrossRef CAS.
63. S. M. Morehouse, *Inorg. Chim. Acta*, 1996, **243**, 327–332 CrossRef CAS.
64. S. S. Massoud, A. A. Gallo, M. J. Dartez, J. G. Gautreaux, R. Vicente, J. H. Albering and F. A. Mautner, *Inorg. Chem. Commun.*, 2014, **43**, 35–38 CrossRef CAS.
65. A. J. Mota, A. Rodríguez-Diéguez, M. A. Palacios, J. M. Herrera, D. Luneau and E. Colacio, *Inorg. Chem.*, 2010, **49**, 8986–8996 CrossRef CAS PubMed.
66. P. J. Hay, J. C. Thiebault and R. Hoffmann, *J. Am. Chem. Soc.*, 1975, **97**, 4884–4899 CrossRef CAS.
67. M. A. Palacios, A. Rodríguez-Diéguez, A. Sironi, J. M. Herrera, A. J. Mota, J. Cano and E. Colacio, *Dalton Trans.*, 2009, 8538–8547 RSC.
68. E. Colacio, J. E. Perea-Buceta, A. J. Mota, E. K. Brechin, A. Prescimone, M. M. Hänninen, P. Seppälä and R. Sillanpää, *Chem. Commun.*, 2012, **48**, 805–807 RSC.

Footnote

† Electronic supplementary information (ESI) available. CCDC 1547618. For ESI and crystallographic data in CIF or other electronic format see I